Astrophys Space Sci
DOI 10.1007/s10509-014-2039-z

ORIGINAL ARTICLE

CUBES: cassegrain U-band Brazil-ESO spectrograph

B. Barbuy · V. Bawden Macanhan · P. Bristow · B. Castilho · H. Dekker · B. Delabre · M. Diaz · C. Gneiding · F. Kerber · H. Kuntschner · G. La Mura · W. Maciel · J. Meléndez · L. Pasquini · C.B. Pereira · P. Petitjean · R. Reiss · C. Siqueira-Mello · R. Smiljanic · J. Vernet

Received: 13 January 2014 / Accepted: 25 June 2014

Abstract CUBES is a high-efficiency, medium-resolution ($R \sim 20{,}000$) ground based UV (300–400 nm) spectrograph, to be installed in the cassegrain focus of one of ESO's VLT unit telescopes in 2017/18. The CUBES project is a joint venture between ESO and IAG/USP, and LNA/MCTI. CUBES will provide access to a wealth of new and relevant information for stellar as well as extragalactic sources. Main science cases include the study of beryllium and heavy elements in metal-poor stars, the direct determination of carbon, nitrogen and oxygen abundances by study of molecular bands in the UV range, as well as the study of active galactic nuclei and the quasar absorption lines. With a streamlined modern instrument design, high efficiency dispersing elements and UV-sensitive detectors, it will give a significant gain in sensitivity over existing ground based medium-high resolution spectrographs, enabling vastly increased sample sizes accessible to the astronomical community. We present here a brief overview of the project including the status, science cases and a discussion of the design options.

Keywords Spectrograph · High spectral resolution

B. Barbuy (✉) · M. Diaz · W. Maciel · J. Meléndez · C. Siqueira-Mello
IAG, Universidade de São Paulo, Rua do Matão 1226, São Paulo 05508-090, Brazil
e-mail: barbuy@astro.iag.usp.br

V. Bawden Macanhan · B. Castilho · C. Gneiding
Laboratório Nacional de Astrofísica, MCTI, Rua Estados Unidos 154, Itajubá, Brazil

P. Bristow · H. Dekker · B. Delabre · F. Kerber · H. Kuntschner · G. La Mura · L. Pasquini · R. Reiss · J. Vernet
European Southern Observatory, Karl-Schwarzschild Strasse 2, 85748 Garching bei München, Germany

C.B. Pereira
Observatório Nacional, Rua José Cristino 77, 20921-400 Rio de Janeiro, Brazil

P. Petitjean
Institut d'Astrophysique, 98bis Bd. Arago, 75014 Paris, France

R. Smiljanic
Nicolaus Copernicus Astronomical Center, ul. Rabiańska 8, 87-100 Toruń, Poland

1 Introduction

In the present era of multiple efforts towards infrared astronomy, only a few spectrographs will be available in the ground-based ultraviolet region (UV). The Cassegrain U-Band Brazilian Spectrograph—CUBES spectrograph is intended to fill this gap.

A predicted gain in sensitivity for this spectrograph over UVES, the main VLT player at the spectral resolution and wavelength, corresponds to about 2 magnitudes at 350 nm, and up to 3 magnitudes at 320 nm. For example, it will be possible to achieve in only 45 min exposure time a S/N ~ 50 per spectral bin at 350 nm for $V = 16$ (G0V template, airmass $= 1.3$, slit-transmission factor $= 0.83$).

In Sect. 2 we present the Galactic science case, and in Sect. 3 the extragalactic case. In Sect. 4 the instrument is described. In Sect. 5 the plans and timescales for building the instrument are given. In Sect. 6 a summary is given.

2 Galactic science case

Metal-poor stars are a major target in UV studies. Because of their long lifetimes, low-mass stars retain in their atmospheres a fossil record of the chemical elements in the in-

Published online: 09 July 2014

terstellar medium at the time of their formation. This enables near-field cosmology. Large surveys such as SDSS and HK/HES are producing a new list of a few thousand such stars with $V < 17$. Studies of planetary nebulae, symbiotic stars, interstellar medium (ISM) and comets also show spectral lines of interest in the UV.

2.1 Beryllium abundances

The UV is the unique spectral window for the determination of beryllium (hereafter Be) abundance with the Be II resonance lines at 313.042 and 313.107 nm. In the following we outline four noteworthy science applications for Be.

2.1.1 Solar twins

In order to test solar models of lithium (Li) depletion, theoreticians require stars that differ only slightly from the Sun in mass, age, rotation and metallicity. Note that this assumption breaks down quickly for solar analogs with masses 10 % higher than solar, because they will develop a convective core, thus changing radically the stellar interior description. Be is important to constrain the mechanisms (e.g. mass, age, convection treatment, extra-mixing mechanisms, mass loss, metallicity) that destroy Li in the Sun and solar twins (Monroe et al. 2013), because it allows independent tests of the models required for Li depletion. The depletion of Be is about one third of the Li depletion (Boesgaard and Krugler 2009) because Be is destroyed at higher temperatures. Solar twins have not been targeted in the past because they are extremely hard to identify. Besides, they are much fainter than solar analogs making them more challenging targets for UV spectroscopy. A recent spectroscopic survey of solar twins (Meléndez et al. 2009) has identified the best sample of solar twins available; they can provide new insights into the apparent anomalies in the solar Li and Be abundances and provide stringent constraints in the modeling of Li and Be depletion.

2.1.2 Mixing and stellar physics

Li abundances have been extensively used in the literature as a way to study mixing between the surface material and the interior of stars. Standard stellar evolution, which only allows for mixing in convective layers, fails to explain nearly all Li abundance patterns observed so far at the surface of low-mass stars. Some of the effects uncovered by the observations are: (1) The vast majority of F- and early G-type stars (including the Sun) deplete Li during the main-sequence (Sestito and Randich 2005), (2) the Li-dip, a strong decrease in Li abundances of main sequence stars in an interval of 300 K around 6700 K (Boesgaard and Tripicco 1986), (3) the presence of a spread of Li among solar-type stars in old clusters like M67 and in field stars (Pasquini et al. 1997), (4) Li dilution starting in subgiants before the first dredge-up (Lebre et al. 1999), (5) the star-to-star scatter in Li and the Li-rotation connection in open clusters and associations both younger and slightly older than the Pleiades (Soderblom et al. 1993). These observations reveal the action of physical processes beyond convection. Many different physical mechanisms have been proposed to explain these observations: atomic diffusion, mass loss, magnetic fields, rotation-induced mixing, mixing by internal gravity waves, or combinations of some of these processes. To help constrain the nature and description of the transport mechanisms of chemicals and angular momentum inside low-mass stars it is important to combine Li data with Be abundances (Smiljanic et al. 2010, 2011).

2.1.3 Be as a cosmochronometer

The single stable isotope ^{9}Be of this element, behaves as a primary element in the early Galaxy and is a pure product of cosmic-ray spallation of heavy (mostly CNO) nuclei in the interstellar medium (Reeves et al. 1970). Assuming cosmic-rays to be globally transported across the Galaxy, the Be production can be considered as a widespread process and its abundance should be rather homogeneous at a given time in the early Galaxy. It should have a smaller scatter than the products of stellar nucleosynthesis. Thus, Be should show a good correlation with time and could be employed as a cosmochronometer for the early stages of the Galaxy (Suzuki and Yoshii 2001; Pasquini et al. 2005). Together with abundances of oxygen (or alpha elements), Be can be used to investigate the evolution of star formation rate in the old Galactic components (halo and thick disk). The idea is to use a diagram of [O/Fe] vs. log(Be/H),[1] as shown in Fig. 1, where the abscissa can be considered as increasing time and the ordinate as the star formation rate. A division of stars into two components can be interpreted as a difference in the time scales of star formation. It is important here to observe main sequence stars with undepleted Li, that also did not deplete their initial Be abundance. For example, the halo stars analyzed in Smiljanic et al. (2009) were shown to split into two components in a diagram of [O/Fe] vs. log(Be/H), revealing two components with distinct star formation histories. Although the right way to interpret this division in two components is still an open question, in a scenario where Be traces time it would indicate that the halo is not a single uniform population with a single age-metallicity relation. The difference may be related to the accretion of external systems or to variations of star

[1] We use the standard notation $[\mathrm{O/Fe}] = \log(\mathrm{O/Fe})_{star} - \log(\mathrm{O/Fe})_{\odot}$; for Be we use instead log (Be/H) that gives the absolute abundance, log A(Be), with respect to that of hydrogen log A(H) = 12.

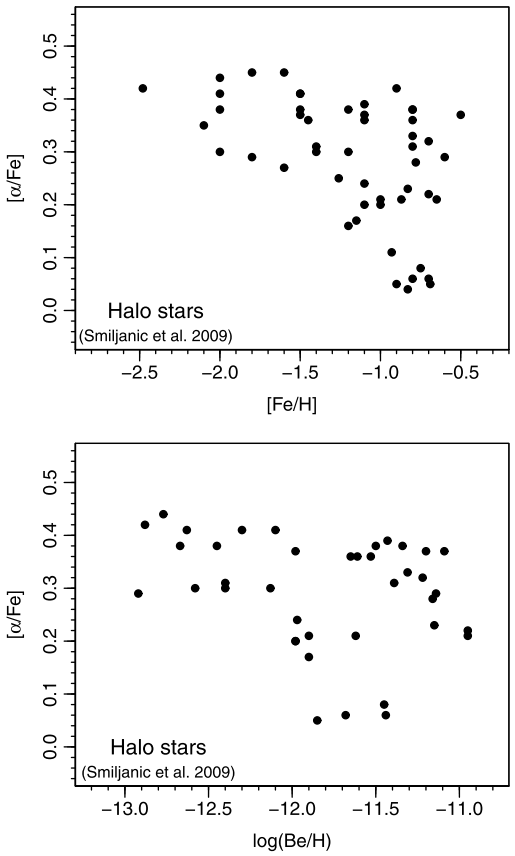

Fig. 1 *Top panel:* The [α/Fe] ratio as a function of metallicity ([Fe/H]) for the halo stars analyzed by Smiljanic et al. (2009). Even though there is a large scatter, the characteristic "knee-like" behavior is seen. *Bottom panel:* The [α/Fe] ratio as a function of the beryllium abundances log(Be/H) for the same stars. In this panel, the stars clearly divide into two sequences

formation in different and initially independent regions of the early halo. The division seems clearer when Be is used as a timescale, instead of [Fe/H], the usual timescale indicator, and Be can thus contribute to improve our knowledge of the Galaxy formation processes (see e.g. Tan and Zhao 2011). Larger samples of kinematically selected metal-poor stars are needed to better understand the detailed behavior of Be in the Galaxy, its use as a cosmochronometer, and as a discriminator of stellar populations. Detections of Be in extremely metal-poor stars ([Fe/H] ~ -3.00) suggest a possible flattening of the relation log(Be/H) vs. [Fe/H], as given in Fig. 2, that could be seen as a plateau (Primas et al. 2000a, 2000b). However, there are only a few stars in this regime with determined Be abundances and other authors have questioned the existence of the flattening (see e.g. Boesgaard et al. 2011). All other known stars with this or lower metallicity are too faint to be observed with current instrumentation.

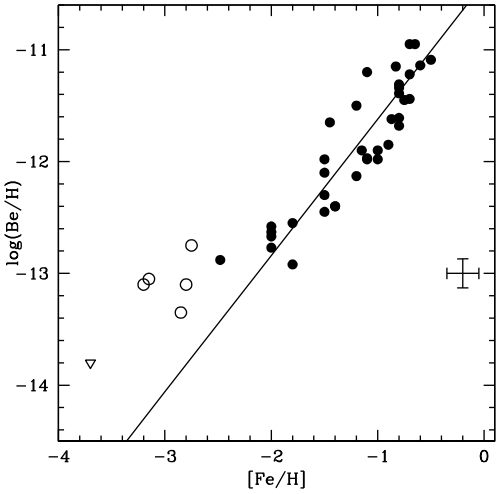

Fig. 2 Beryllium abundances as a function of metallicity. The stars analyzed by Smiljanic et al. (2009) are shown as *solid circles*, the extremely metal-poor stars re-analyzed by Smiljanic et al. (2012) are shown as *open circles*. Also shown as an *open triangle* is the upper limit of the Be abundance for star BD+44 493 determined by Ito et al. (2009). The *open circles* seem to suggest a deviation from the linear relation between Be and Fe that could indicate a flattening

2.1.4 Be and the formation of globular clusters

All the globular clusters (GS) analyzed with sufficient depth so far show signs of chemical inhomogeneities in the light elements (Li, C, N, O, Na, Mg, and Al; see e.g. Gratton et al. 2004). These manifest as typical signatures of material processed by proton-capture reactions. It is now accepted that this material was produced by a previous generation of stars that polluted those that are observed now, although the nature of these polluters is still debated (massive AGBs or fast-rotating massive stars; see e.g. Decressin et al. 2007; Ventura and D'Antona 2009). In this context Li and Be are of particular interest as they are fragile, destroyed in (p, α) reactions in temperatures above $\sim 2.5 \times 10^6$ K and $\sim 3.5 \times 10^6$ K, respectively. Li, however, can be produced in AGB stars via the Cameron-Fowler mechanism while Be is never produced, only destroyed. As the other proton-reactions (CNO and NeNa cycles) require much higher temperatures, the processed material is completely devoid of Be, regardless of the polluter. In NGC 6397, stretching the UVES capabilities, Pasquini et al. (2004) observed two turn-off stars with much different O and possibly the same Be. In the simple dilution-pollution scenarios currently proposed to explain the chemical properties of globular clusters, Be should always be diluted in O-poor stars, since it is only present in primordial material, not in processed material. If this result could be confirmed, then the current scenario of GC second generation of star formation would have to be abandoned. CUBES will enable Be determinations in several clusters with different populations, and characteristics,

e.g. NGC 6397, NGC 6752, M4, ω Cen, NGC 2808, among others.

2.2 Heavy-elements in metal-poor stars

The site for r-element production is still unknown (e.g. Thielemann et al. 2011). The best way to try to solve this question is the observation of heavy elements in old metal-poor stars, which retain in their atmospheres the ejecta of supernovae at early times. In the wavelength region 300–400 nm to be covered by CUBES, there are many strong lines of the species Y II, Zr II, Nb II, Ru I, Rh I, Pd I, Ag I, Sn I, La II, Ba II, Ce II, Nd II, Sm II, Eu II, Gd II, Tb II, Dy II, Er II, Tm II, Ho II, Os I, Yb II, Lu II, Hf II, Os I, Ir I, Pb II, Pr II, Th II. There are also unique abundance indicators from lines of elements such as Bi and U: U II 385.957 nm, Bi I 302.4635 and 306.7 nm (the latter however severely blended). The heaviest radioactive elements U and Th, measured with respect to each other, or to elements produced in the same nucleosynthesis events, such as Bi, can be used to derive the stellar age (e.g. Barbuy et al. 2011). Germanium is also an important nucleosynthesis r-process indicator, through a unique measurable line at Ge I 303.907 nm (e.g. Siqueira-Mello et al. 2013). The abundances of Ge in particular can be used to deduce the dominance of s-process or r-process nucleosynthesis in metal-poor stars.

The study of nucleosynthesis in supernovae can be constrained by the ratios of abundances of elements from the first ($38 < Z < 48$), second ($56 < Z < 73$) and third ($76 < Z < 88$) heavy-element peaks, and the actinides ($Z > 89$). Therefore the derivation of heavy-element abundances is one of the most useful topics to be addressed with a UV spectrograph.

2.3 C,N,O in metal-poor stars

The elements carbon, nitrogen, and oxygen are the most abundant after hydrogen; and carbon and oxygen are the first abundant elements to be formed by nucleosynthesis after H and He. Consequently, they are key elements in studies of the chemical evolution of the Galaxy and galaxies in general, as well as in studies of stellar evolution. The main nitrogen indicator used in the literature are CN bands, among which the strongest ones are in the near-UV, in particular CN(0,0) at 388.3 nm. For the use of CN, one has to previously derive C, available in the optical from the CH G-bandhead at 431 nm or a weak C(0,0) bandhead at 563.5 nm. In the near-UV there is the unique available strong NH bandhead at 336 nm. The NH band measurement in important samples would allow a direct measurement of nitrogen (e.g. Pasquini et al. 2008). Oxygen also has important indicators in the near-UV, several strong OH lines occurring around 330 nm. In metal-poor turn-off dwarf stars, only these OH lines are strong to be measurable in these stars. Therefore the situation regarding CNO is: with C measured in the optical, generally from the CH G-bandhead at 431 nm, it is then used to derive N from CN bandheads, the strongest ones found in the near-UV. Nitrogen is even better derived, directly from UV NH bandheads, the strongest of which is at 336 nm. Note that there are discrepancies between the CN and NH indicators that need to be better understood. This was clearly pointed out by Spite et al. (2005), where N abundances from the CN bandhead at 388.3 nm were 0.4 dex higher than those derived from NH 336 nm bands. Oxygen abundances can be derived from 4 sets of lines: (i) the forbidden [OI] 630.031, 636.379 nm lines measurable in giants of [Fe/H]> -3.0; (ii) the permitted OI 777.196, 777.418 and 777.540 nm lines, and the weaker triplet at 615.603, 615.680 and 615.817 nm, measurable in dwarfs and subgiants, or in supergiants; (iii) the ultraviolet (UV) OH lines (AX electronic transition); (iv) the infrared (IR) OH lines (X vibration-rotation transition). The importance of the near-UV OH lines applies mainly to metal-poor turn-off dwarf stars, in which these OH lines are the only of the lines listed above, that are strong enough to be measurable in these stars. More studies of NH and OH lines are needed in terms of line lists and molecular constants, and this basic aspect could be one of the first aims related to CUBES.

2.4 Other stellar cases

2.4.1 Planetary nebulae in the UV

Accurate chemical abundances of several elements that can be difficult to study in stars can be obtained from emission lines of planetary nebulae (PN), especially concerning the elements He, C, N, O, Si, S, and Cl. Apart from optical and infrared lines, several of these lines are in the ultraviolet. In the range 300–400 nm several important emission lines can be measured in PN, mostly collisionally excited lines such as [O II] 372.6, 372.9, O III 302.3, 304.3, 313.3, [Ne III] 386.9, [Ne III] 334.3, 387.0, 396.7, 396.8, [N II] 306.3, [N I] 346.7, [S III] 372.2, 379.8, [Cl II] 358.7, 367.8, [Cl III] 334.3, 335.4, [Cl IV] 311.9, 320.4, [Ar III] 300.6, 311.0 nm. These lines can be used to determine the ion abundances of the corresponding elements and the electron temperature in the case of the [O II] line, especially when other optical (or infrared) lines are available. Some Bower fluorescence lines can be produced in specific environments, including O III 313.3, 334.1 and 344.4. Some recombination lines of abundant elements are also often observed, such as O III 326.5, He I and H8 388.9, Hϵ 397.0 nm. At effective temperatures in excess of 30000 K, the PN central stars emit most of their radiation in the ultraviolet, peaking around 120 nm, with measured radiation

up to about 320 nm. There are over 2000 planetary nebulae known in our Galaxy, with many more observed in the galaxies of the Local Group, especially in M31 and the Magellanic Clouds. Presently, there are relatively accurate abundances measured for a few hundred Galactic nebulae, which will constitute the main initial targets for the UV studies (see for example Milanova and Kholtygin 2009; Stanghellini et al. 2005). Also, recent studies of the central stars based on UV measurements have given a powerful insight into the strong stellar winds observed in these stars, particularly those that are H deficient, both for the Galaxy and the Magellanic Clouds (Herald and Bianchi 2004a, 2004b; Keller et al. 2011). The above science does not set stringent requirements on the spectral resolution, but the measurement of emission line abundances requires a reasonably accurate flux calibration. In other words, abundances are usually derived from line fluxes measured relative to Hβ, leading to the electron temperatures and densities, from which the abundances are calculated. In order to obtain a typical uncertainty of 0.10–0.20 dex for the abundances, the line fluxes have to be accurate down to a few tenths of the Hβ flux.

2.4.2 *Bowen effect in symbiotic stars, PN, AGN, and X-ray binaries*

For a long time (Bowen 1934, 1935), it has been recognized that some OIII permitted emission lines seen in planetary nebulae (PN) are produced essentially by the so-called Bowen fluorescence mechanism. This mechanism consists in the excitation of O III by the Lyα line of He II at 303.78 nm (in a remarkable coincidence transitions of O III rest respectively at 303.80 and 303.69 nm). Subsequent cascades yield the main Bowen lines, and further decays from those levels create the subordinate lines. The subordinate lines can also be excited by other processes, such as charge transfer of OIV in collision with neutral hydrogen and/or radiative and dielectronic recombination (Liu et al. 1993). As a consequence of Bowen fluorescence several emission lines can be detected between 310 nm and 410 nm and between 370 and 570 nm. Therefore, the study of Bowen lines in symbiotic stars and other gaseous nebulae can be useful to probe the physical conditions under which these lines are formed and also measurements of the Bowen efficiency can be compared with photo-ionization models.

2.4.3 *Novae, close binaries, compact stars and symbiotic stars*

In the following we outline several science opportunities which arise from CUBES in the area of close binaries, compact stars and symbiotic stars.

1. Precision accretion column tomography using weak high ionization lines: Magnetically funneled mass transfer in close binaries can be studied using tomographic reconstructions of the gas flow by measuring emission line profiles along the orbit. High ionization metal lines like N IV 347.9, 348.3, 348.5 nm are expected to be weak. However, their profiles may reveal the column structure close to the accreting white dwarf, probing the presence of magnetic quadrupoles. Dozens of potential targets are available in the southern hemisphere.

2. Transient Heavy Element Absorption Systems in Novae: Short-lived absorption line systems were recently discovered in recent high-resolution observations of classical novae outbursts (Williams et al. 2008) while probing the circumbinary medium around classical novae using Transient Heavy Element Absorption (THEA). Single ionized lines of Sc, Ti, V, Cr, Fe, Sr, Y, Zr, and Ba are possibly formed in a circumbinary gas. Chemical abundances and mass loss rates in this gas are essential to the understanding of binary evolution and production of SNIa in those systems. Many of these lines can be conveniently observed in the UV range, beyond the Balmer jump in emission. Two to six classical and recurrent novae per year are expected to present measurable THEA systems.

3. Velocity structure of neon lines in recurrent novae: The presence of strong neon lines in recurrent novae is an indication of a CV (cataclysmic variable) SNIa progenitor. The evolution of the UV NeIII and NeV line profiles and flux can be used as a constraint to 3D photo-ionization models of the nova shell. Such models provide the best estimate of the mass loss in outbursts defining the evolution of the white dwarf close to the Chandrasekhar limit. The kinematics and mixing of neon in the ejecta is key to understand how nova outbursts change along time as the white dwarf gravity increases. Recurrent novae are rare systems—about 20 objects are currently known. U Sco has strong neon lines and regular recurrences every 10 years.

4. White dwarfs—spectral signatures of planets or small bodies accretion: High resolution and high S/N observations of the blue and UV continuum of white dwarfs may reveal the presence of metals with a short diffusive time-scale indicating recent accretion of material of planetary/asteroid origin as seems to be the case in GD 362 (Jura et al. 2009). The observation of metal lines in the UV has advantages regarding the absence of Zeeman-split components and brighter continuum. Precise atmospheric density diagnostics for those WD of the DA type can be also made in the UV by using the Inglis-Teller method. The search for suitable planet accreting WDs candidates can be pursued by taking into account their infrared and X-ray properties.

3 Extragalactic science case

The science opportunities for the proposed UV spectrograph for extragalactic targets most notably involves the study of

Table 1 Target properties. Based on the Catalogue of Quasars and AGNs (Véron-Cetty and Véron 2010)

Class	n°	$z_{\min}$	$z_{\max}$	$V_{\min}$	$V_{\max}$
Seyfert 1	206	0.001	0.240	12.72	18.00
Intermediate	1382	0.003	0.268	11.79	18.00
Seyfert 2	717	0.001	0.270	9.04	18.00
LINER	390	0.001	0.141	9.25	16.50
QSO	3743	0.016	4.545	10.16	18.00
BL Lac	109	0.023	1.72	12.81	18.00
Unclassified	376	0.001	0.127	10.83	16.50

active galactic nuclei and quasar absorption line systems. Table 1 gives expected numbers of observable AGNs and QSOs.

3.1 Active galactic nuclei in the UV

Active Galactic Nuclei (AGN) are characterized by different observational properties. In general, they share very powerful non-stellar energy sources (10^{40} erg s$^{-1} \leq L \leq 10^{48}$ erg s^{-1}), emitting their signal over a broad range of frequencies, from radio waves up to X- and γ-rays. When the nuclear source is observed along a nearly unobscured line of sight, it usually dominates the emission, sometimes completely outshining the host galaxy. If, on the contrary, there is severe absorption towards the nucleus, the central source can be obscured, but its influence on the close environment becomes more evident. The former configuration corresponds to what is called a Type 1 object, while the latter is named a Type 2 source, within a spectroscopic classification scheme devised on the basis of the optical-UV observational properties (Osterbrock and Dahari 1983; Antonucci 1993). A characteristic signature of AGN spectra is the excess of ionizing radiation, associated with the Big Blue Bump, a sharp rise of the SED at a rest frame wavelength $\lambda \leq 400$ nm, which covers the UV domain, probably extending up to soft X-ray energies (Elvis et al. 1994). This feature makes the UV range of AGN naturally interesting. It is directly visible in the spectra of Type 1 sources, while in Type 2 objects its presence can be inferred by the properties of several recombination lines, triggered by the large amount of ionizing photons associated with the bump (Veilleux and Osterbrock 1987; Kewley et al. 2006). Its origin has not yet been fully established, but it is believed to arise from thermal emission in the accretion disk which is feeding on the gravitational field of the central Super Massive Black Hole (SMBH).

AGN spectra in the UV regime are rich in emission lines. The most commonly reported near-UV detections involve bright nebular emission lines from [Ne V] 3426, [O II] 3727,3729, [Ne III] 3868, as well as some recombination lines of H and He I. However, there are significant differences in the intensity ratios, especially of nebular and recombination lines, among Type 1 and 2 spectra, because of the distinct regions where the bulk of line emission comes from. Some of these lines, especially those of [Ne V] and [O II], act as indicators of the ionization conditions in the line emitting plasma and they can be used to track obscured AGN activity (Heckman 1980; Gilli et al. 2010). Since the currently available spectral coverage of their wavelength range is marginal, most of the work devoted to these spectral features involves objects whose emission lines are brought closer to the optical domain, via cosmological redshift. This is a remarkable concern, because observations at high redshift are typically biased towards the brightest sources. Therefore, a comparison with the properties of local objects becomes fundamental to account for possible selection effects and cosmic evolution.

Besides the spectral features mentioned above, the near-UV window includes several contributions of great importance for the investigation of AGN. In the low redshift domain, the limit of the hydrogen Balmer series falls in this wavelength range, while, looking at higher redshift objects, broad emission and absorption features, strictly connected to the nature of the unresolved nuclear source, enter the near-UV frequencies. In order to point out the contributions resulting from the analysis of these properties, it is convenient to discuss them according to their different origin.

3.1.1 The narrow line region

The emission lines that we commonly observe in AGN spectra can be classified in two categories: broad lines, with FWHM $\geq 10^3$ km s^{-1}, and narrow lines, with FWHM $\leq 10^3$ km s^{-1}. They originate from two distinct regions, characterized by different physical properties. The Narrow Line Region (NLR) is filled by a tenuous plasma (10^3 cm$^{-3} \leq N_e \leq 10^4$ cm^{-3}), ionized by the energetic output of the AGN central engine, through a combination of photo-ionization and shock processes, whose signature is left in diagnostic emission lines, such as [Ne V] 3426, [O II] 3727,3729, [Ne III] 3869, Hβ, [O III] 4959,5007, [N II] 6548,6583, Hα, and [S II] 6716,6731 (Solórzano-Iñarrea et al. 2001). In nearby objects the NLR can be resolved and it is often observed to have a conical, or bi-conical morphology, with an axis of symmetry which, in the case of strong radio emission, lies along the direction of the radio axis (e.g. Wilson and Tsvetanov 1994). The main property, which distinguishes the NLR gas from other nebular environments, such as planetary nebulae, is the source of ionization, that involves a different radiation field, with respect to the case of a hot star, and some contribution from shock fronts (Moy and Rocca-Volmerange 2002). The result is that NLR spectra may exhibit a wide range of relative line intensities, reflecting the role played by the various ionizing factors. Indeed,

investigating the properties of nebular environments is one of the most successful fields of astrophysical spectroscopy and the NLR of active galaxies represents an attractive target. The relative strengths of emission lines originated by a single element in different ionization configurations, not frequent in the optical domain, but available in near-UV for [Ne V] and [Ne III], are sensitive to the source of gas ionization, and they can be used to distinguish among radiation and shock processes. Resolving the profiles of these emission lines and combining them with observations of other species, such as [O II], provides further details concerning the gas kinematical and chemical configuration, which are crucial to understand the origin of the NLR gas and its role within the host galaxy.

3.1.2 The broad line region

In contrast to the narrow emission lines, the broad lines appear exclusively in Type 1 AGN spectra and they are not generally found in correspondence with forbidden atomic transitions. Some exceptions are possible in the profiles of the brightest features, such as [O III] 495.9, 500.7 nm. The most prominent broad emission lines include Lyα 121.6, C IV 154.9, C III] 190.9, Mg II 279.8 nm, the Fe II multiplets, He II 468.6, He I 587.6 nm, and the Balmer, Paschen, and Brackett series of H, in the optical and IR wavelength ranges. In several cases, the far UV lines, especially Lyα, as well as the lines from C IV, C III], and Mg II, are strong enough to be clearly detectable in high redshift objects, where they are observed at near UV-optical frequencies. However, the observation of these lines in the optical domain implies the exploration of redshifts in the range of $0.6 \leq z \leq 2.7$, where intrinsic source brightness selection effects are certainly significant. Studying these lines in the near-UV regime allows us to explore considerably closer sources ($z = 0.25$ is high enough to observe Mg II, while $0.83 \leq z \leq 1.88$ is still needed to detect the C and Ly spectral features), with clear advantages both in terms of selection efficiency and in the understanding of the object evolution through different cosmological epochs. Indeed, these UV lines, together with Hβ in the optical domain, provide the best established tracers of the dynamical effects arising from the SMBH gravitational field (e.g. Vestergaard and Peterson 2006). Several arguments confirm a strong interaction between the continuum source and the BLR (Blandford and McKee 1982; Wandel et al. 1999). Moreover, the detection of Type 1 spectral features in the polarized signal of some Seyfert 2 galaxies reveals the existence of an intrinsically Type 1 spectrum, reflected onto the observational line of sight by a directly illuminated medium, located away from the obscuring material that surrounds the nucleus (Antonucci and Miller 1985). The BLR unresolvable structure, however, places severe uncertainties on the determination of the central engine physical properties from the analysis of the emission lines. It is worth recalling that we have only marginal knowledge of the actual ionizing radiation SED and of its influence on the line emission process (Elvis et al. 1994; Mullaney and Ward 2008), this is among the main problems that need to be solved. Furthermore, some heavy ions, especially Fe II, are contributing to the optical-UV bands with complex line multiplets, which require a spectral resolution of $R \geq 15{,}000$, in order to clarify their origin. It is estimated that Fe II emission line multiplets can account for a significant fraction of the total energy processed in the BLR plasma (up to $\sim$50 %, Joly 1987) and they are part of the strongest relationship existing among the spectral properties of different Type 1 AGN (Boroson and Green 1992). Fe II multiplets are found from the far UV regime all the way down to optical frequencies (Baldwin et al. 2004), but their properties in the near UV still have to be thoroughly explored. The case for a complete understanding of this important contribution to the BLR spectrum is further stressed by the circumstance that such an ion cannot survive direct exposure to the AGN radiation field. Its presence constrains the BLR self-shielding capability, which is a fundamental tool to penetrate the structure and dynamics of matter within the innermost core of AGN (Ferland et al. 2009). Therefore, a new scientific instrument with $R \sim 20{,}000$, appropriately devised to analyze the near UV regime, will play a major role in further developing these topics.

3.1.3 AGN circum-nuclear environment

It is often observed that the circum-nuclear regions of active galaxies, within a distance $r \approx 1$ kpc from the AGN, have significantly different properties, with respect to quiescent systems. Several investigations have found evidence of young stellar populations, indicating that relatively recent star formation activity occurred in the nuclear regions of active galaxies (González Delgado et al. 2001; Rafanelli et al. 2009). Analysis of the near-UV regime at a spectral resolution $R \sim 20{,}000$ becomes particularly attractive in the case of the circum-nuclear regions of nearby low luminosity AGN and Seyfert 2 galaxies (Cid Fernandes et al. 2001). It has been pointed out that the stellar populations of these objects share an excess of intermediate-age stars. The existence of absorption features, corresponding to the high-order Balmer lines, and the shape of the Balmer and two-photon continuum constrain their recent star formation history. The signature of recent star formation is statistically relevant even in relatively low spatial resolution observations ($\sim 1''$–$3''$), but bringing together better spectral and spatial resolution capabilities represents a fundamental goal.

3.1.4 Absorption systems

In spite of the dominant role played by emission line plasmas in the spectra of AGN, several absorption features bring a relevant contribution to our understanding of the underlying physics. The strongest absorption lines are associated with the resonance transitions of the most common ions and, since they involve the fundamental levels of the electron configuration, they typically fall in the far-UV regime. It is estimated that a fraction of approximately 10 % of QSOs exhibit broad absorption lines, most often associated with UV lines of the BLR spectrum, such as Lyα 121.6 and C IV 154.9 nm. Their systematic blueshift, with respect to the local rest frame, suggests an origin in outflowing winds covering a small range of inclinations, on the border of the obscuring structure which distinguishes among Type 1 and Type 2 objects. Spectropolarimetric observations support this picture, detecting on average a larger degree of polarization in the continuum and, above all, in the absorption troughs of broad absorption line sources, with respect to normal Type 1 objects, pointing towards an enhanced contribution from light scattering in the resulting spectrum (Schmidt and Hines 1999; Ogle et al. 1999). Since a spectral resolution of $R \sim 20{,}000$ is fundamental to probe the kinematical configuration of the absorbing material, the optimized near-UV sensitivity offered by CUBES will significantly increase the number of sources where such observations can be carried out.

3.2 Quasar absorption line systems

The blue end of the optical wavelength range is of utmost importance for the study of:

- the intergalactic medium at intermediate redshifts ($z \sim$ 1.5–2), its physical state (temperature, ionization) but also its metal content (through OVI), and
- the interstellar medium of high redshift galaxies and in particular its molecular content (H_2 for $z > 2$; CO for $z > 1$).

Specific projects include:

3.2.1 The intergalactic medium at $z = 1.5$–2

The gas traces the potential wells of the dark matter and its large-scale structures. The IGM is therefore seen as a smooth pervasive medium which is the reservoir of baryons for galaxy formation. In turn, because of feedback processes, galaxy formation is imprinted on the properties of the IGM.

The properties of the IGM have been well studied at redshift larger than $z \sim 2$ (e.g. Theuns et al. 1998), whereas lower redshifts to be reachable in the UV are complementary.

The IGM contains a fairly large amount of metals, revealed in particular by CIV and OVI absorptions. The OVI transitions at 103.1 and 103.7 nm are redshifted in the very blue part of the optical spectrum for $z > 2$. The properties of these metals and their spatial location are barely understood because CIV and OVI do not seem to follow each other well and there seems to be a large fraction of IGM absorbers with large oxygen abundances (Schaye et al. 2003). The origin of this pollution by stars is therefore unclear (Pop III objects or winds from primordial galaxies). Here, $R \sim 20{,}000$ and again high sensitivity in the blue are well suited.

3.2.2 The ionizing background at $z = 1.5$–2

It is well known that the characteristics of the Lyman-α forest change in the vicinity of the quasar due to the additional ionizing flux emitted by the quasar itself. The mean neutral hydrogen fraction decreases when approaching the quasar. It is possible to use this effect, together with knowledge of the quasar luminosity and its position, to derive the mean flux of the UV background. In this way, it is possible to probe the presence of overdensities associated with the quasar (Guimarães et al. 2007). Using pairs of quasars would allow investigating the transverse proximity effect.

3.2.3 The galaxy-IGM interaction

The interplay between galaxies and the IGM is a key element in understanding galaxy formation. The IGM is the reservoir of baryons for galaxy formation and galaxies accrete warm gas from the IGM along the filaments of large-scale structures. In turn, feedback processes that return energy and material back to the IGM from the galaxy population are needed to explain the colors and the luminosity function of present-day galaxies (Bower et al. 2006). Indeed, winds from star-forming galaxies have been detected (Adelberger et al. 2003). These processes can be explored by studying the correlation between galaxies (or quasars for the transverse proximity effect) and the absorptions detected along QSO lines of sight in the same field. These issues can also be investigated by observing quasar lines of sight in fields where galaxies have been surveyed. In particular it would be very interesting to correlate the metal absorption lines with the positions of the galaxies (Scannapieco et al. 2006). At large redshift ($z > 2.5$), there is an excess of HI absorption compared to the mean within ~5 Mpc of a typical L* Lyman break galaxy. It is however unclear whether this excess holds up to the galaxy itself or if there is less HI absorption close to the galaxy (<1 Mpc) due to the effect of feedback, due to star formation activity, ionizing flux and injection of kinematic energy from supernovae. For these galaxies, it would be most interesting to search for associated OVI absorption that could reveal galactic

winds. In addition, these studies could be extended to redshifts corresponding to the peak of the star formation activity in the universe. CUBES is a very interesting instrument for these issues because it would allow the study of these effects at lower redshift and the detection of OVI in Lyman break galaxies. Most importantly fainter quasars (compared to UVES) can be targeted in the few deep fields where a tremendous amount of information is already available.

3.2.4 The interstellar medium of high-z galaxies

Although molecular hydrogen is a prominent constituent of the interstellar medium in galaxies, it is rarely detected directly. In emission, only excited H_2 is detected and only absorption can allow us to derive physical properties of the standard diffuse molecular medium. The first systematic search for molecular hydrogen in high-redshift ($z_{abs} > 1.8$) DLA galaxies was carried out using UVES at the VLT (Noterdaeme et al. 2008) and discovered 13 H_2 systems. Using refined selection criteria including the results of this survey and the use of CI absorption, it is possible to increase the efficiency of the selection of H_2 bearing systems to about 30 %. Applying these criteria to the SDSS database yields a sample of candidates for the detection of molecules. H_2 is now routinely detected although the number of systems that can be observed is limited by the sensitivity of the instrument. In addition CO has been discovered together with several HD absorbers (Srianand et al. 2008). These detections open up the exciting possibility to study astro-chemistry at high redshift. H_2 transitions are found deep in the blue and the proposed spectrograph can be considered as the ideal instrument to study the diffuse molecular ISM at high redshift because of both the sensitivity and the resolution. It will be possible to go fainter and to hit the bulk of the population.

A summary of interesting lines in extragalactic objects, and corresponding redshifts is given in Table 2. More complete line lists can be found, for example, in Morton et al. (1988), Morton (1991).

Table 2 Examples of important lines in AGN Narrow line (NLR) and Broad line regions (BLR), and QSO absorption lines to be observed in the UV, and corresponding redshifts

Target	Lines	Redshifts
AGN-NLR	NeV 342.6	$0 < z < 0.1$
	OII 372.7, 372.9	$0 < z < 0.02$
AGN-BLR	MgII 280	$0.07 < z < 0.36$
	Lyα121.5	$1.46 < z < 2.13$
	CIV 154.9	$0.94 < z < 1.45$
	CIII 190.9	$0.35 < z < 0.6$
QSO	ZnII 202.5, 206.2	$0.45 < z < 0.98$
	CrII 205.5, 206.1, 206.5	$0.45 < z < 0.85$
	Lyα121.5	$1.46 < z < 2.13$
	Lyβ102.5, OVI103.7	$1.89 < z < 2.70$
	MgII 280	$0.07 < z < 0.36$
ISM-cold gas	HI, H_2 (∼100 lines)	$1.46 < z < 2.13$
	CI 165, SiII150.6	$0.81 < z < 1.52$
	OI 130.2, CII133.4	$1.25 < z < 1.92$
	FeII 260	$0.15 < z < 0.46$
ISM-warm gas	SiIII120.6, SiIV129.3	$1.32 < z < 2.15$
	OVI103.7	$1.89 < z < 2.66$
	CIV 154.9	$0.94 < z < 1.45$
	NV124.2	$1.42 < z < 2.06$

4 Instrument overview

The aim of the CUBES design is to produce a simple, streamlined instrument that avoids the introduction of mechanisms, modes and multiplexing capabilities that are not strictly necessary. The CUBES science case can be well addressed with an instrument that is much less complex than other 2nd generation VLT instruments. Less complex means quicker to design and build whilst being less vulnerable to risk. This in turn implies an instrument that is cheaper to build and easier to operate and calibrate. X-shooter is an example of an instrument that, apart from having three spectrographs specialized to their respective bands, is otherwise a relatively straightforward point and shoot spectrograph and this is probably one of the secrets of its success.

CUBES will interface with the VLT environment at a Cassegrain focus and hence benefit from the 8 m primary mirror and the efficient operations model of the VLT. However, it will also be subject to the UV extinction at Paranal (Fig. 3) and occupy a focus that is in considerable demand. The latter issue has led us to pursue a design that enables rapid mounting and dismounting of the instrument so that it can be used in campaign mode, periodically vacating the focus for use by other instruments.

There are three fundamental requirements for CUBES that drive the design:

- CUBES shall significantly improve upon throughput (and signal-to-noise) of existing ground based UV spectrographs. This is of particular importance below 330 nm where the atmospheric transmission at Paranal drops sharply.
- CUBES shall achieve $R \geq 20{,}000$
- CUBES shall provide access to the wavelength range 310–360 nm (with a goal of 302–385 nm)

The resolution requirement of $R \geq 20{,}000$ was the result of a large number of spectral synthesis calculations of specific lines in metal-poor stars, at various resolutions. Resolution has to be traded against wavelength coverage: the higher the resolution, the larger is the required detector area

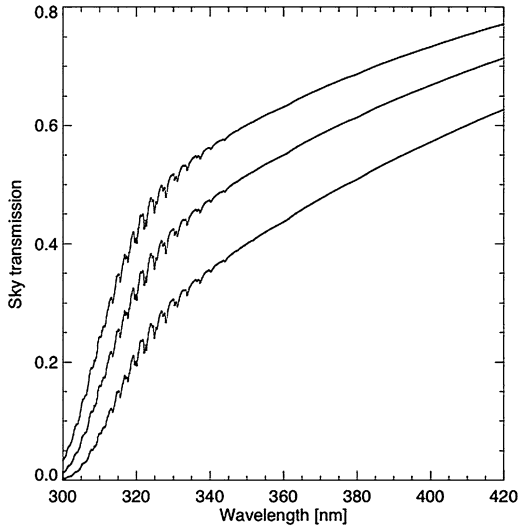

Fig. 3 Atmospheric transmission at the Paranal VLT platform (Noll et al. 2012). From top to bottom, the curves correspond to airmass = 1.0, 1.3 and 1.8. Note that the transmission drops sharply with wavelength below 330 nm and is 15–20 % lower at airmass = 1.8 than at zenith across most of the wavelength range in the plot

Table 3 Choices arising from top level requirements

Design aspect	Implications
Cassegrain	Flexure away from zenith
Slicer (no AO)	Complexity of A&G DRS; Noise
No pre/cross-dispersion	Resolution vs. Wavelength range
Minimal surfaces	Difficulty/cost of optics
High-efficiency grating	New technology/cost
High QE detector	New technology/cost
Ground based/Paranal	Atmosphere

Acronyms: AO: adaptive optics; A&G: acquisition & guiding; DRS: data reduction software; QE: quantum efficiency

and the size of the grating, hence cost and complexity. Other choices were constrained by technology. The top level requirements (TLRs) led to choices and implications summarized in Table 3. Further details can be found in the Phase A report at http://www.eso.org/sci/meetings/2013/UVASTRO/1_VLT-TRE-ESO-13800-5679_i1_CUBES_SciCase.pdf.

As regards the lower wavelength limit, the requirement for the bluest limit for CUBES is given by the Be line at 313 nm, and to take into account the radial velocity limits implies a blue limit of 310 nm for the spectrograph. If possible to achieve the goal for 302 nm, this will allow the detection of Germanium lines at 302.4 nm and 303.9 nm, besides OH lines, such as the OH $A^2\Sigma(0,0)$ bandhead at 306 nm.

The throughput requirement in particular has led to the following design choices:

- *Cassegrain focus:* The Cassegrain focus at the VLT has a throughput of 77 %, the Nasmyth has only 65 %. A difference with respect to the Nasmyth, where a derotator can be used, mounting at Cassegrain means that the entire optical system will be susceptible to flexure at high airmasses.
- *Image slicer:* Without effective AO in the UV, a slicer is the only way to get medium to high resolution with a realistically sized instrument without incurring high slit-losses. A slicer complicates the guide camera optics and data reduction and incurs a noise penalty since the signal will be spread over more pixels.
- *No cross- or pre-dispersion:* Compared to an efficient first-order grating, a cross-dispersed echelle would have an average efficiency that is lower by 40 %. However, dispensing with cross/pre-dispersion together with the principle of reducing complexity (i.e. avoiding the introduction of multiple optical configurations that access different wavelength ranges) leave us with a direct trade off between resolving power (the second fundamental requirement) and wavelength range (the third fundamental requirement) for a given detector array length. Clearly our first priority is to obtain the longest array length possible by simply arranging as many CCDs as the budget will allow in a long narrow train. However the budget is finite, so the search for the optimum compromise between wavelength range and resolution drives many other aspects of the design and is also the principle reason that we did not consider $R \gg 20{,}000$.
- *Minimum number of surfaces:* An obvious means to reduce transmission losses is to minimize the number of optical interfaces and reflections.
- *High efficiency grating and high QE detectors:* The slit, the grating and the detectors are by far the dominant sources of inefficiency in the optical system. We are investigating state-of-the-art technologies in order to achieve very high efficiencies throughout the wavelength range and in particular below 330 nm (see the next section).

Together these measures facilitate a considerable improvement in efficiency in the UV relative to existing VLT spectrographs as illustrated by Fig. 4. Note that the curves in the figure are all valid for a 1″ slit width. In practice UVES, HIRES and HDS typically operate with a smaller slit width to achieve higher resolution and hence a lower efficiency. It may be that the use of ETC data for the VLT instrument efficiencies leads to unfavorable results since ESO ETCs tend to be rather conservative, in particular UVES is probably much closer to HIRES than Fig. 4 would suggest. Moreover, since all of the other spectrographs are cross-dispersed, the curves represent the envelopes defined by the peak efficiencies in each order, in practice the efficiency achieved in between peaks may be somewhat lower depending upon how well order overlap is handled.

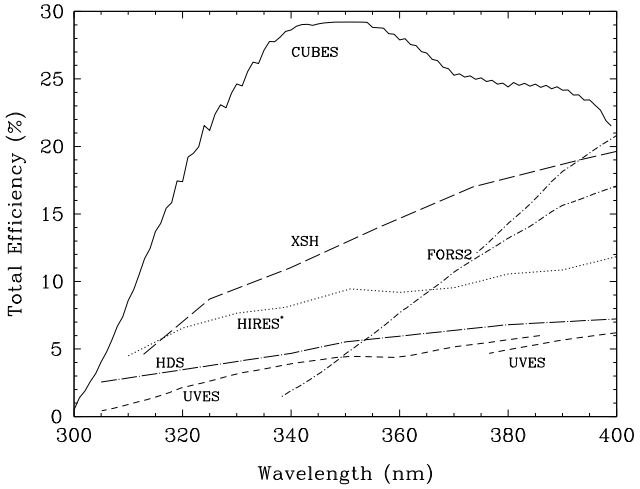

Fig. 4 Predicted efficiency of CUBES including atmosphere, telescope, slit losses, optical system and detector compared to other ground based spectrographs operating in the UV. FORS2 (FORS2 exposure time calculator http://www.eso.org/observing/etc/bin/gen/form?INS.NAME=FORS+INS.MODE=spectro), UVES (UVES exposure time calculator http://www.eso.org/observing/etc/bin/gen/form?INS.NAME=UVES+INS.MODE=spectro) and X-shooter (X-shooter exposure time calculator http://www.eso.org/observing/etc/bin/gen/form?INS.NAME=X-SHOOTER+INS.MODE=spectro) efficiencies were calculated with the instrument ETCs. HIRES (HIRES/Keck efficiency measurements http://www2.keck.hawaii.edu/inst/hires/throughput.html) and HDS (HDS/Subaru efficiency measurements http://www.naoj.org/Observing/Instruments/HDS/efficiency.html) efficiencies were inferred from information appearing on their respective web sites. Note that the HIRES curve has been adjusted upwards by a factor of 1.5 to account for the larger primary mirror of Keck relative to VLT and Subaru, as such it is not strictly a percentage

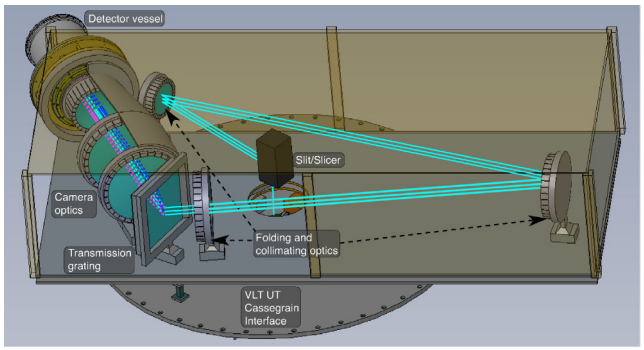

Fig. 5 The CUBES optical bench

The resulting preliminary opto-mechanical design for CUBES is illustrated in Fig. 5. The beam entering from the Cassegrain focus (below in this view) is sliced and collimated before being diffracted by the transmission grating (rectangular component), then focused by the sequence of camera lenses onto the detector (in the dewar at the top left). Table 4 lists the key design parameters. CUBES is in most respects a classical long slit spectrograph which relies upon some state-of-the-art components to achieve exceptional performance.

Table 4 Key CUBES parameters

Slicer	No. slices ≥ 7
	slitlet widths $\leq 0.3''$
Transmission grating	$\sim$3200 mm^{-1}
	1st order
	Ruled width $\sim$260 mm
	Transmission > 80 % @ 320 nm
Detector array	4×4 K $\times$ 2 K $\times$ 15 µm $\times$ 15 µm
	250 mm $\times$ 30 mm
	QE > 85 % @ 320 nm
	Dark current < 0.001e-/pix/s
	RON < 2.5e-
Wavelength range	302–390 nm (TBC)
Resolving power	$\geq$20,000

5 Technical challenges

Three components of CUBES will be critical in order to achieve high efficiency. In this section we describe our efforts to implement them.

5.1 Grating

The preliminary optical design for CUBES employs a transmission grating manufactured using direct write electron-beam lithography (E-beam). This technology, first applied in astronomy for the Gaia project (Zeitner et al. 2010), has a huge potential for the realization of high-performance gratings with higher efficiencies and lower wave-front errors than can be achieved via conventional ruling/replication techniques or holography, especially in the UV and NIR.

Fraunhofer Institut für Angewandte Optik und Feinmechanik, has supplied sample gratings produced with e-beam lithography. Measurements confirm that the samples have an efficiency close to the design predictions, offering $>$20 % improvement over gratings in existing UV spectrographs. The practical challenges of scaling up to a full size grating are currently being investigated. On the VLT, the resolution-slit product of a spectrograph with a 200 mm collimated beam (which is the maximum size that we consider practical for reasons of flexure and weight) and a first-order grating having about 3500 l/mm, will be on the order of 7000. This implies that $R = 20{,}000$ will be achieved only with a slit of around 0.3 arcsec, so to avoid slit losses one needs image slicing.

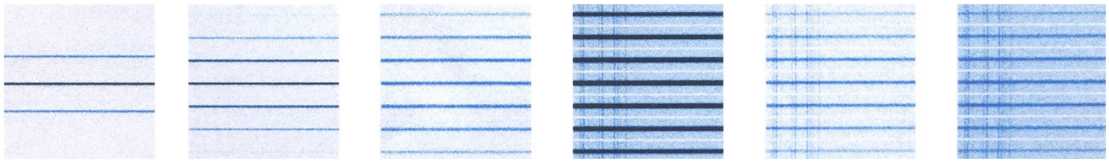

Fig. 6 Sections of simulated raw 2D data. (**a**) G0V source, $B = 14$, 300 s exposure, 0.6 seeing, 30.45 slitlets; (**b**) as (**a**) but with a 70.25 slitlets; (**c**) as (**b**) but for 1.2 seeing; (**d**) as (**c**) but for a 3600 s exposure; (**e**) as (**d**) but for a $B = 19$ QSO; (**f**) as (**e**) but with a darker sky

5.2 Slicer

Clearly increasing the number of slices available to sample the source PSF increases the resolution without significantly reducing the efficiency. Moreover, since there will be no cross-dispersion, there will be ample space for spectra from many slices across the detectors. However this comes at a price of potentially degraded signal to noise because the signal will be spread across more pixels.

We are investigating the signal to noise implications for various numbers of slices of differing widths with the use of 2D simulated data created following the methods described in Bristow et al. (2011). Our initial study considered:

Two realistic target spectra, $V = 19$ QSO and a $B = 14$ G0V star, observed with exposures of 10 s, 300 s and 3600 s, in $0.6''$, $0.8''$, $1.0''$ and $1.2''$ seeing, and sky background spectra scaled appropriately for Paranal dark time and grey time, with 1×1, 1×2, 2×2 and 2×4 pixel binning, assuming a flat field S/N of 200, 500 and 1000, with dark current and readout noise matching the maximum design specification, and 4 slicer set ups ($3 \times 0.45''$, $5 \times 0.35''$, $7 \times 0.25''$, $7 \times 0.35''$). In each case the spectrograph parameters were adapted to ensure that the eventual resolution delivered was the same.

We extracted 1D spectra from the simulated 2D observations and measured the SNR in the continuum around 320 nm. Preliminary results indicate that the effect of spreading the signal over more pixels is not all that significant even for simulations with the fainter target. However this is a work in progress, in particular we need to characterize the dependency upon assumed dark current and readout noise.

If these findings are confirmed then this suggests that we should adopt a slice width of ≤ 0.3 and ≥ 7 slices. A design similar to that used by MUSE (Laurent et al. 2007) would enable this. Figure 4 shows some examples of the simulated 2D raw data for different slicer designs, observing parameters and targets.

5.3 Detector

Advances in coating technologies provide the potential to improve upon the quantum efficiency of detectors employed in the current generation of UV spectrographs. Figure 7 shows the first result from an investigation into the use of state-of-the-art coatings in order to realize very high UV QE devices that meet CUBES requirements carried out at UA Imaging Technologies Laboratory. The measured result for this initial attempt (with an STA0510 CCD, 1200×800 15 µm pixels) already comes very close to satisfying the QE specification of CUBES and there is some optimism that the shortfall below 320 nm can be addressed in subsequent attempts.

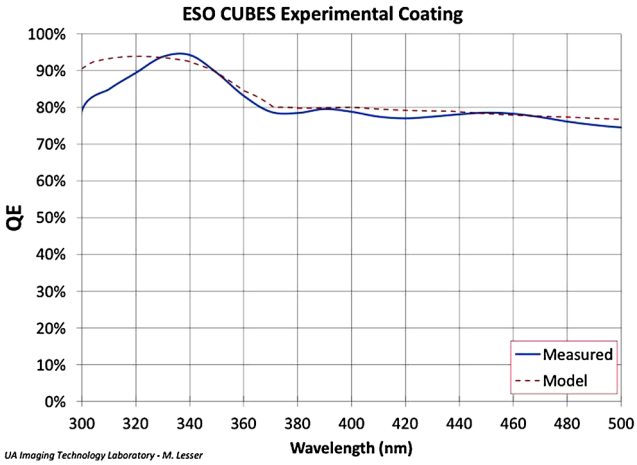

Fig. 7 Detector QE achieved in early tests

5.4 ADC and polarimetric facility

A polarimetric facility is not included because (a) spectropolarimetry would require adding a large number of functions and motors: an insertable analyzer (1 motor), a quarter-wave plate (1), a half-wave plate (2) and a spinning depolarizer (2) after the slicer—a total of 6 additional functions; (b) a slicer will significantly affect the polarization state so the scheme for polarimetry would be to insert an analyzer (e.g. Savart plate) before the slicer that splits the image of the object in "S" and "P" images along the slit direction that are separated by a few arcseconds. However, due to the presence of atmospheric dispersion the position of these images on the entrance aperture will vary with wavelength and zenith distance, complicating the extraction and analysis. (c) Also, the height of the entrance aperture of the slicer is likely insufficient for good spectropolarimetry and sky subtraction in the

presence of atmospheric dispersion, so spectropolarimetry would be limited to small zenith distances only, thereby limiting its usefulness, unless an ADC would be implemented; (d) Finally, the influence of an ADC (which has tilted surfaces) and the slicer (which has at least one 45-degree mirror and possibly further tilted surfaces) on the polarization measurements is likely to be complex and difficult to correct for. In order to maximize throughput, an ADC is not included in the design; the plan is to observe at the parallactic angle so the atmospheric dispersion is aligned with the slit direction.

In conclusion, although spectropolarimetry capability would be desirable to help a limited fraction of science cases, the limitation of the possible results due to more important requirements and the requirements of simplicity, repeatability and efficiency ruled out this option at least at this phase of the project.

6 Summary

Within ESO capabilities, CUBES is complementary to ESPRESSO, that does not cover wavelengths below 380 nm. It is complementary to UVES by reaching 3 magnitudes deeper at 320 nm. It is also complementary to X-shooter in terms of resolution.

The main technical issues presently are the prototyping of the grating, and detector coatings and the design of the slicer. After a Phase A study, the project was approved in September 2012.

The construction of the instrument is conditional to the ratification of Brazilian government to accession of Brazil to ESO. CUBES is expected to be completed in 2017/18.

Acknowledgements We are grateful to Sebastian Deiries and Olaf Iwert for advice regarding detector systems and Mike Lesser for investigating state-of-the-art detector coatings in the CUBES wavelength range.

References

Adelberger, K.L., et al.: Astrophys. J. **584**, 45 (2003)
Antonucci, R.: Annu. Rev. Astron. Astrophys. **31**, 473 (1993)
Antonucci, R., Miller, J.S.: Astrophys. J. **297**, 621 (1985)
Baldwin, J.A., et al.: Astrophys. J. **615**, 610 (2004)
Barbuy, B., Spite, M., Hill, V., et al.: Astron. Astrophys. **534**, 60 (2011)
Blandford, M.D., McKee, C.F.: Astrophys. J. **255**, 419 (1982)
Boesgaard, A.M., Krugler, J.: Astrophys. J. **691**, 1412 (2009)
Boesgaard, A.M., Tripicco, M.J.: Astrophys. J. **303**, 724 (1986)
Boesgaard, A.M., et al.: Astrophys. J. **743**, 140 (2011)
Boroson, T.A., Green, R.F.: Astrophys. J. Suppl. Ser. **80**, 109 (1992)
Bowen, I.S.: Publ. Astron. Soc. Pac. **46**, 146 (1934)
Bowen, I.S.: Astrophys. J. **81**, 1 (1935)
Bower, R.G., et al.: Mon. Not. R. Astron. Soc. **370**, 645 (2006)
Bristow, P., et al.: Understanding the behaviour of X-shooter via the application of a physical model. Exp. Astron. **31**(131), 156 (2011)
Cid Fernandes, R., et al.: Mon. Not. R. Astron. Soc. **355**, 273 (2001)
Decressin, T., et al.: Astron. Astrophys. **464**, 1029 (2007)
Elvis, M., et al.: Astrophys. J. Suppl. Ser. **95**, 1 (1994)
Ferland, G., et al.: Astrophys. J. **707**, L82 (2009)
Gilli, R., et al.: Astron. Astrophys. **519**, 92 (2010)
González Delgado, R.M., Heckman, T., Leitherer, C.: Astrophys. J. **546**, 845 (2001)
Gratton, R.G., Sneden, C., Carretta, E.: Annu. Rev. Astron. Astrophys. **42**, 385 (2004)
Guimarães, R., et al.: Mon. Not. R. Astron. Soc. **377**, 657 (2007)
Heckman, T.M.: Astron. Astrophys. **87**, 152 (1980)
Herald, J.E., Bianchi, L.: Astrophys. J. **609**, 378 (2004a)
Herald, J.E., Bianchi, L.: Astrophys. J. **611**, 294 (2004b)
Ito, H., Aoki, W., Honda, S., Beers, T.C.: Astrophys. J. **698**, L37 (2009)
Joly, M.: Astron. Astrophys. **184**, 33 (1987)
Jura, M., et al.: Astrophys. J. **699**, 1473 (2009)
Keller, G.R., Herald, J.E., Bianchi, L., Maciel, W.J., Bohlin, J.C.: Mon. Not. R. Astron. Soc. **418**, 705 (2011)
Kewley, L.J., et al.: Mon. Not. R. Astron. Soc. **372**, 961 (2006)
Laurent, F., et al.: Innovative slicer design and manufacturing (2007). SPIE Proc. 6273-90
Lebre, A., et al.: Astron. Astrophys. **345**, 936 (1999)
Liu, X., Danziger, J., Murdin, P.: Mon. Not. R. Astron. Soc. **262**, 699 (1993)
Meléndez, J., et al.: Astrophys. J. **704**, L66 (2009)
Milanova, Yu.V., Kholtygin, A.F.: Astron. Lett. **35**, 518 (2009)
Monroe, T., et al.: Astrophys. J. **774**, L32 (2013)
Moy, E., Rocca-Volmerange, B.: Astron. Astrophys. **383**, 46 (2002)
Morton, D.C., York, D.G., Jenkins, E.B.: Astrophys. J. Suppl. Ser. **68**, 449 (1988)
Morton, D.C.: Astrophys. J. Suppl. Ser. **77**, 119 (1991)
Mullaney, J.R., Ward, M.J.: Mon. Not. R. Astron. Soc. **385**, 53 (2008)
Noll, S., et al.: An atmospheric radiation model for Cerro Paranal. Astron. Astrophys. **543**, A92 (2012)
Noterdaeme, P., Ledoux, C., Petitjean, P., Srianand, R.: Astron. Astrophys. **481**, 327 (2008)
Ogle, P.M., et al.: Astrophys. J. Suppl. Ser. **125**, 1 (1999)
Osterbrock, D.E., Dahari, O.: Astrophys. J. **273**, 478 (1983)
Pasquini, L., Randich, S., Pallavicini, R.: Astron. Astrophys. **325**, 535 (1997)
Pasquini, L., et al.: Astron. Astrophys. **426**, 651 (2004)
Pasquini, L., et al.: Astron. Astrophys. **436**, L57 (2005)
Pasquini, L., et al.: Astron. Astrophys. **489**, 315 (2008)
Primas, F., et al.: Astron. Astrophys. **364**, L42 (2000a)
Primas, F., et al.: Astron. Astrophys. **362**, 666 (2000b)
Rafanelli, P., et al.: New Astron. Rev. **53**, 186 (2009)
Reeves, H., et al.: Nature **226**, 727 (1970)
Scannapieco, et al.: Mon. Not. R. Astron. Soc. **365**, 615 (2006)
Schaye, J., et al.: Astrophys. J. **596**, 768 (2003)
Schmidt, G.D., Hines, D.C.: Astrophys. J. **512**, 125 (1999)
Sestito, P., Randich, S.: Astron. Astrophys. **442**, 615 (2005)
Siqueira-Mello, C., Spite, M., Barbuy, B., et al.: Astron. Astrophys. **550**, 122 (2013)
Smiljanic, R., Pasquini, B., Bonifacio, P., et al.: Astron. Astrophys. **499**, 103 (2009)
Smiljanic, R., et al.: Astron. Astrophys. **510**, A50 (2010)
Smiljanic, R., et al.: Astron. Astrophys. **535**, A75 (2011)
Smiljanic, R., Pasquini, L., Bonifacio, P.: ASP Conf. Ser **458**, 79 (2012)
Soderblom, D., et al.: Astron. J. **105**, 2299 (1993)
Solórzano-Iñarrea, C., Tadhunter, C.N., Axon, D.J.: Mon. Not. R. Astron. Soc. **323**, 965 (2001)
Spite, M., Cayrel, R., Plez, B., et al.: Astron. Astrophys. **430**, 655 (2005)
Srianand, R., et al.: Astron. Astrophys. **482**, L39 (2008)

Suzuki, T.K., Yoshii, Y.: Astrophys. J. **549**, 303 (2001)
Stanghellini, L., Shae, R.A., Gilmore, D.: Astrophys. J. **622**, 294 (2005)
Tan, K., Zhao, G.: Astrophys. J. **738**, L33 (2011)
Theuns, T., et al.: Mon. Not. R. Astron. Soc. **301**, 478 (1998)
Thielemann, F.-K., et al.: Lecture Notes in Physics, vol. 812, p. 153. Springer, Berlin (2011)
Veilleux, S., Osterbrock, D.E.: Astrophys. J. Suppl. Ser. **63**, 295 (1987)
Ventura, P., D'Antona, F.: Astron. Astrophys. **499**, 835 (2009)
Véron-Cetty, M.-P., Véron, P.: Astron. Astrophys. **518**, 10 (2010)
Vestergaard, M., Peterson, B.M.: Astrophys. J. **641**, 689 (2006)
Wandel, A., Peterson, B.M., Malkan, M.A.: Astrophys. J. **526**, 579 (1999)
Williams, R.E., et al.: Astrophys. J. **685**, 451 (2008)
Wilson, A.S., Tsvetanov, Z.I.: Astron. J. **107**, 1227 (1994)
Zeitner, U.D., Fuchs, F., Kley, E.B.: High performance dielectric gratings for space applications (2010). Proc. SPIE 8450E, 84502Z